

## Reduced order modelling of a flow around an airfoil with a changing angle of attack<sup>\*)</sup>

W. STANKIEWICZ<sup>1)</sup>, M. MORZYNSKI<sup>1)</sup>, R. ROSZAK<sup>1)</sup>,  
B. R. NOACK<sup>2)</sup>, G. TADMOR<sup>3)</sup>

<sup>1)</sup> *Poznan University of Technology*  
*Institute of Combustion Engines and Transportation*  
*Piotrowo 3, 60-965 Poznań, Poland*  
*e-mail: stankiewicz@stanton.ice.put.poznan.pl*  
*morzynski@stanton.ice.put.poznan.pl*  
*roszak@stanton.ice.put.poznan.pl*

<sup>2)</sup> *Technische Universität Berlin*  
*Institut für Strömungsmechanik und Technische Akustik (ISTA)*  
*Müller-Breslau-Strasse 11, D-10623 Berlin, Germany*  
*e-mail: Bernd.R.Noack@TU-Berlin.DE*

<sup>3)</sup> *Northeastern University*  
*Department of Electrical & Computer Engineering*  
*Communications and Digital Signal Processing (CDSP) Center*  
*440 Dana Building*  
*360 Huntington Avenue, Boston, MA 02115-5000, U.S.A.*  
*e-mail: tadmor@ece.neu.edu*

MODEL REDUCTION BASED on Galerkin projection is a key technique used in feedback flow control. It significantly accelerates the flow computations, and thus it can be suitable for the aeroelastic simulations or, generally, in the flow analysis of changing configurations and boundaries. The present paper concerns the reduced-order Galerkin modelling of 2D flow around NACA-0012 airfoil, with angle of attack changing from  $\alpha = 30^\circ$  to  $\alpha = 45^\circ$ . It emphasizes the requirements of simplicity and accuracy of reduced order models (ROMs) used in control applications and discusses possible mode bases. Finally, it describes the constructed model, based on the modes resulting from Proper Orthogonal Decomposition (POD) and the novel technique of continuous mode interpolation. This method allows smooth transition between different operating and boundary conditions and allows the design of least-dimensional Galerkin model for control purposes.

### 1. Introduction

FLUID FLOW IS THE CAUSE of a number of phenomena, that significantly influence the efficiency of designed products. The reduction of undesirable separation

---

<sup>\*)</sup>The paper was presented at XVIII Polish Conference of Fluid Mechanics (KKMP), Jastrzębia Góra, 21–25 September, 2008.

or turbulence, leading to aerodynamic drag increase, flutter, reduction of lift force, etc., is possible by means of flow control techniques. Such control may be passive or active.

Passive control requires no external energy source and is usually based on the modification of flow domain with splitter plates, control wires, wake disruptors or riblets, what influences the vortex generation [1, 2].

Active control utilizes external energy sources – the actuators. If the actuation is independent of the state of the flow, it is called open-loop control. In feedback (closed-loop) flow control the actuation is based on the up-to-date state of the flow, measured by a certain number of sensors placed in the flow domain. The data from the sensors is processed by a controller, that requires some kind of mathematical model of the flow.

While the accuracy and the dimension of the model determine the utility of the control, neither black-box models nor Navier–Stokes equations (1.1) can be used in real applications requiring accurate flow prediction,

$$(1.1) \quad \partial_t \mathbf{u} + \nabla \cdot (\mathbf{u} \otimes \mathbf{u}) + \nabla p - \frac{1}{\text{Re}} \Delta \mathbf{u} = 0.$$

The discretized Navier–Stokes equations can be considered as a high-dimensional model, containing thousands or millions of degrees of freedom. Real-time control requires very short time (the order of milliseconds) between sensing the flow state and the actuation. It is impossible to solve the high-dimensional flow model in such a short time.

To overcome this problem, low-dimensional models, containing only a few degrees of freedom, are used.

The aim of present work is to construct a low-dimensional model of flow around an airfoil with changing angle of attack.

One of the most commonly used techniques of model reduction is the Galerkin method [3, 4], described in Sec. 3. Possible mode bases for low-dimensional Galerkin modelling are discussed in Sec. 4. Section 5 provides the description of Proper Orthogonal Decomposition, used to compute empirical modes for the chosen test-cases.

The desired model, useful in such time-consuming flow analyses as optimization of passive control, aircraft maneuver analysis or fluid-structure interaction computations, must be able to adapt to varying operating and boundary conditions of the flow. The key technique for such an adaptation is continuous mode interpolation [5, 6], presented in Sec. 6. Reduced Order Models (ROMs) of flow around the airfoil with changing angle of attack  $\alpha$ , using POD modes and continuous mode interpolation, are presented in Sec. 7.

## 2. Test-case problem description

In this study, the flow around well-known NACA-0012 airfoil is considered. Small value of Reynolds number and large angles of attack have been chosen to make the vortex street apparent. Due to small Reynolds number ( $Re \approx 45$ , related to the chord length), Direct Numerical Simulation (DNS) [7] and following POD decompositions are performed on two-dimensional meshes. For each angle of attack used, they have the same number of degrees of freedom (DOFs) and topology. These finite element meshes are obtained by the spring-deformation [8] of initial grid for  $\alpha = 30^\circ$  (Fig. 1).

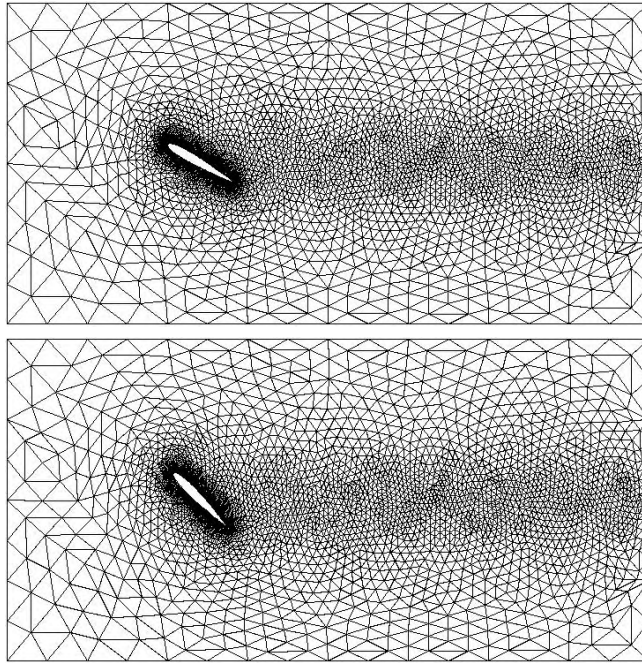


FIG. 1. Top: computational domain for  $\alpha = 30^\circ$ , discretized with Finite Element Method (initial mesh). Bottom: deformed mesh used in design of model GM-2 ( $\alpha = 45^\circ$ ).

Initial conditions describe steady flow at  $\alpha = 30^\circ$ . The uniform stream is horizontal, defined on left, top and bottom boundaries of the domain. These conditions are set to secure the repeatability of the results regardless the software used. Small disturbance of velocity on the boundary of airfoil (set for  $t \leq 1$ ) enforces the transition to periodic flow and limit-cycle oscillations (LCO) (Fig. 2, top).

Next, for  $500s \leq t \leq 510s$ , the angle of attack increases to the value of  $\alpha = 45^\circ$ . This change affects the coherent structures appearing in the flow (Fig. 2, bottom).

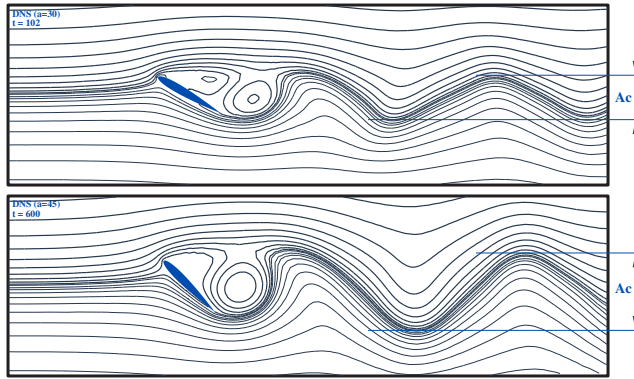


FIG. 2. The streamlines of periodic flow at  $\alpha = 30^\circ$  (top) and  $\alpha = 45^\circ$  (bottom).

New limit-cycle oscillations are characterized by different values of period size, kinetic energy of disturbance, shift-mode amplitude, etc. All these parameters are compared with previous state ( $\alpha = 30^\circ$ ) in Table 1.

**Table 1. The comparison of flow properties for limit cycle oscillations and two values of angle of attack.**

Angle of attack	$\alpha = 30^\circ$	$\alpha = 45^\circ$
Time the LCO is reached	$t_{LCO1} \approx 65$ s	$t_{LCO2} \approx 550$ s
Period size	$T = 6.85$ s	$T = 8.22$ s
Kinetic energy of the disturbance	TKE = 2.66	TKE = 4.69
Central streamline amplitude	$A_C = 62\%$ chord length	$A_C = 107\%$ chord length
Shift-mode amplitude	$a_{\text{shift}} = 2.839$	$a_{\text{shift}} = 5.377$

Shift-mode, defined as a difference between steady solution and a mean flow, is used to stabilise the reduced-order model [4].

### 3. Galerkin method

Model reduction of the flow shown in previous section is based on the assumption that the state of flow  $\mathbf{u}$  can be approximated by a base flow  $\mathbf{u}_0$  (e.g. steady or mean solution) and a sum of products of modes  $\mathbf{u}_j$  and Fourier coefficients  $a_j$ , describing the disturbance (3.1):

$$(3.1) \quad \mathbf{u}^{[N]} = \mathbf{u}_0 + \sum_{j=1}^N a_j \mathbf{u}_j = \sum_{j=0}^N a_j \mathbf{u}_j, \quad a_0 \equiv 1.$$

Due to the use of finite number of modes  $N$ , the right-hand-side of approximated Navier–Stokes equation is equal to residual  $R^{[N]}$  (3.2):

$$(3.2) \quad \partial_t \mathbf{u}^{[N]} + \nabla \cdot (\mathbf{u}^{[N]} \otimes \mathbf{u}^{[N]}) + \nabla p^{[N]} - \frac{1}{\text{Re}} \Delta \mathbf{u}^{[N]} = R^{[N]}.$$

The Fourier coefficients in every time step can be computed after projection of approximated Navier–Stokes equation onto the space spanned by selected modes (so-called Galerkin projection). In Hilbert space, it is done by the computation of inner products of residual  $R^{[N]}$  and each of the modes  $\mathbf{u}_i$ , and equating them to zero (3.3). The inner product is affected by the (varying) computational domain:

$$(3.3) \quad (\mathbf{u}_i, R^{[N]})_\Omega = \int_\Omega \mathbf{u}_i R^{[N]} d\Omega = 0.$$

This approach leads to the system of ordinary differential equations (Galerkin System) (3.4), linking the Fourier coefficients  $a$ , their time derivatives  $\dot{a}$  and constant parameters  $l_{ij}$  and  $q_{ijk}$  (3.5):

$$(3.4) \quad \dot{a}_i = \frac{1}{\text{Re}} \sum_{j=0}^N l_{ij} a_j + \sum_{j=0}^N \sum_{k=0}^N q_{ijk} a_j a_k,$$

where:

$$(3.5) \quad l_{ij} = (\mathbf{u}_i, \Delta \mathbf{u}_j)_\Omega \quad \text{and} \quad q_{ijk} = -(\mathbf{u}_i, \nabla \cdot (\mathbf{u}_j \otimes \mathbf{u}_k))_\Omega$$

are the results of Galerkin Projection of appropriate terms of approximated Navier–Stokes equations.

Following B. R. NOACK, P. PAPAS and P. A. MONKEWITZ [9], pressure term  $-\nabla p$  is dependent on Fourier coefficient values, so  $p$  can be derived from Poisson's equation (3.6):

$$(3.6) \quad \Delta p = -\nabla \cdot (\mathbf{u} \cdot \nabla) \mathbf{u}.$$

Galerkin projection of this term leads to surface integral (3.7):

$$(3.7) \quad (\mathbf{u}_i, -\nabla p)_\Omega = - \oint_{\partial\Omega} \mathbf{u}_i p dA.$$

As was noticed by B. R. NOACK, P. PAPAS and P. A. MONKEWITZ [10], in case of absolutely unstable wake flows and arbitrarily large domains the pressure term can be neglected. Such a situation occurs for the cases analysed in this paper.

#### 4. Possible mode bases

The set of modes used for low-dimensional modelling can be obtained mathematically, physically or empirically (Table 2) [9].

The examples of mathematical modes are solutions of the carrier-field ansatz [11], generalised streamfunctions [11, 12], spectral methods based on Fourier decomposition and Chebyshev polynomials [13], or wavelets [14].

**Table 2. Galerkin models for Navier–Stokes equations. An ‘X’ denotes that Galerkin approximation is affected by property [9].**

Galerkin method	computational	traditional		
modes	local (e.g. FEM)	global		
		math.	physical	empirical
boundary conditions	X	X	X	X
continuity equation		X	X	X
Navier–Stokes eq.			X	X
flow data				X
model dimension	high	med.	med.- low	low
grid dependence	X	independent		

They do not depend on Navier–Stokes equation or flow data, and the only required information is geometry of domain and boundary conditions. The utility of these modes is reduced to the configurations with high symmetry, like the Taylor–Couette equation or canal flow [15], due to high computational costs and a large number of modes required to represent real flow.

Physical modes can be divided into eigenmodes of the Stokes problem [16, 17], singular Stokes modes [18] and eigenmodes of linearised Navier–Stokes equations (eigenmodes of global stability analysis) [19, 20]. All of these modes incorporate the information from linearised Navier–Stokes equations, geometry of domain and boundary conditions.

Physical modes resulting from global stability analysis usually are not sufficient to construct accurate Galerkin models of wake flows [21], but they can be used to improve the dynamical properties of more advanced models: extrapolated and with continuous mode interpolation [4, 6, 21].

Empirical modes are based on the experimental data or unsteady solutions of Navier–Stokes equations, and are obtained from Proper Orthogonal Decomposition (also known as Karhunen–Loève Decomposition) [22–24]. POD modes are optimal in energy representation by construction, so they possibly better

describe the Navier–Stokes attractor (limit-cycle oscillations of periodic flow) than the same number of modes obtained in any different manner [15]. Better description means similar shapes of coherent structures and levels of disturbance kinetic energy.

The description of the POD decomposition and modes computed for flow around NACA-0012 airfoil at different angles of attack are presented in Sec. 5.

## 5. Proper Orthogonal Decompositions for various angles of attack

Empirical modes resulting from Proper Orthogonal Decomposition [25] are the most widely used ones in the area of reduced-order modelling. The method is based on the assumption, that there is a correlation between successive snapshots  $\mathbf{v}_i$  of the flow.

The first step in POD is the computation of time-averaged solution  $\bar{\mathbf{u}}$

$$(5.1) \quad \bar{\mathbf{u}} = \frac{1}{M} \sum_{m=1}^M \mathbf{v}_m.$$

Resulting vectors  $\dot{\mathbf{v}}_i$  describe the fluctuations in the flow. This data is required to compute the autocorrelation matrix  $C$  of size  $N \times N$ :

$$(5.2) \quad C = \frac{1}{M} S S^T, \quad \text{where } S = [\dot{\mathbf{v}}_1, \dot{\mathbf{v}}_2, \dots, \dot{\mathbf{v}}_M].$$

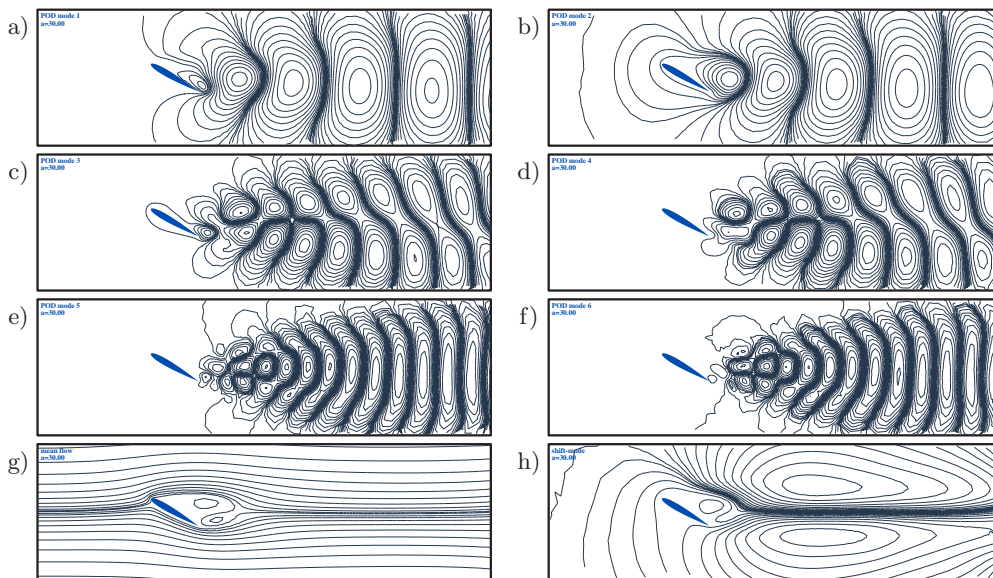


FIG. 3. The streamlines of six most energetic POD modes (a)–(f), mean flow (g) and shift-mode (h) for  $\alpha = 30^\circ$ .

Next, the vectors describing flow fields are centered

$$(5.3) \quad \hat{\mathbf{v}}_m = \mathbf{v}_m - \bar{\mathbf{u}}, \quad m = 1, \dots, M.$$

Eigenvectors  $\mathbf{u}$  of standard eigenproblem  $C\mathbf{u} = \lambda I\mathbf{u}$ , related to eigenvalues  $\lambda$  of largest magnitude, are the POD modes used in model reduction.

In the present work, POD modes were computed using snapshot technique of SIROVICH [26], basing on two distinct sets of vectors (describing limit-cycle oscillations of flow for  $\alpha = 30^\circ$  and  $\alpha = 45^\circ$ ). In both cases, snapshots describing ten flow periods have been used.

In the case of flow at  $\alpha = 30^\circ$  (Fig. 3), first two POD modes represent 94.11% of the disturbance kinetic energy (TKE), and 99.85% of TKE in the case of first 6 modes.

Similar results are obtained for the second value of angle of attack (Fig. 4). In this case, first 2 POD modes represent 96.21% of TKE, and first 6 POD modes – again 99.85% of TKE.

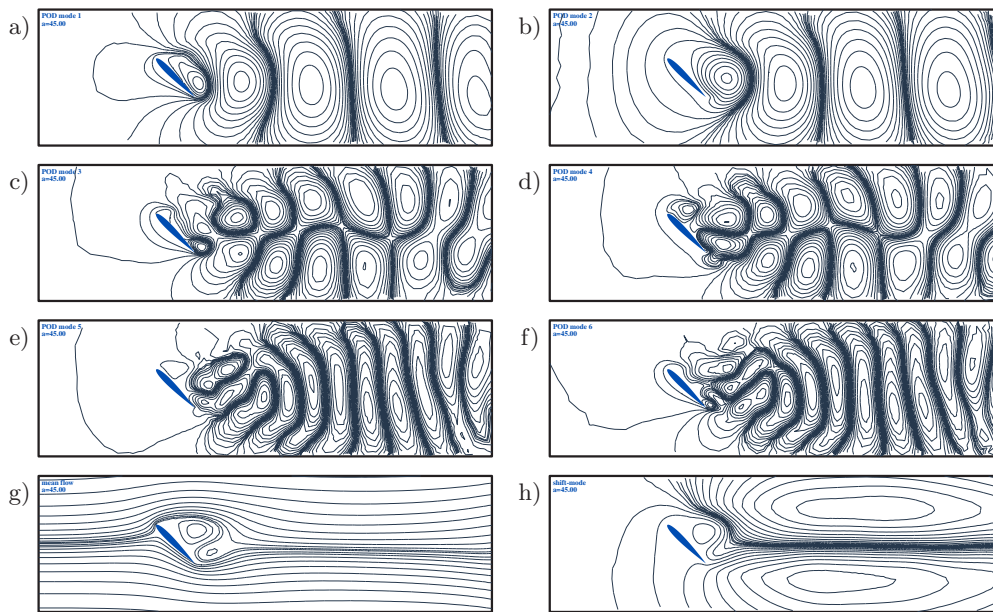


FIG. 4. The streamlines of six most energetic POD modes (a)–(f), mean flow (g) and shift-mode (h) for  $\alpha = 45^\circ$ .

Characteristic wave number of the first pair of POD modes is 1.2 times smaller when compared with the decomposition of flow for  $\alpha = 30^\circ$ , and the wave number of the second pair of modes is 1.34 times smaller. It means that for smaller angle of attack there are more vortices apparent per unit length.

## 6. Continuous mode interpolation

DNS and Proper Orthogonal Decomposition of flows for  $\alpha = 30^\circ$  and  $\alpha = 45^\circ$  shows the differences in arising vortex streets. For both operating conditions, coherent structures represented by POD modes slightly differ in wave numbers and fluctuation envelopes. Different values of TKE and period sizes (Table 1) result in the change of amplitudes and frequencies of Fourier coefficients (Fig. 5).

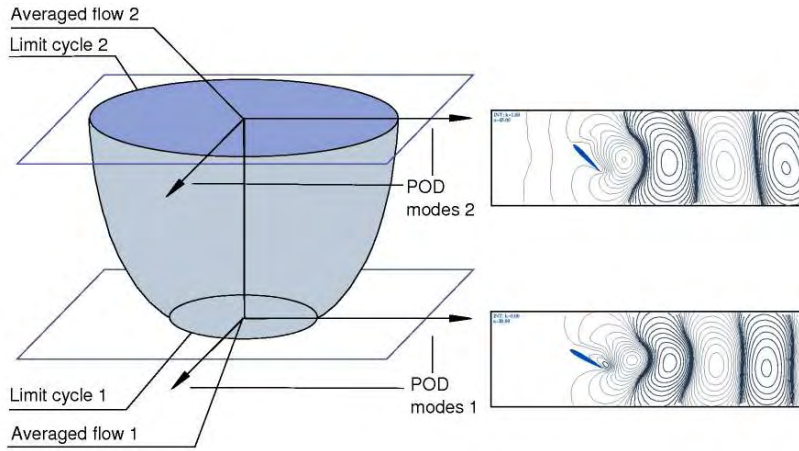


FIG. 5. Principal sketch of the wake dynamics of transition between two operating conditions:  $\alpha = 30^\circ$  and  $\alpha = 45^\circ$ . Right-hand side illustrates vortex streets for limit cycles on the mean-field paraboloid (left).

The use of POD modes computed for inappropriate flow state results in inaccurate prediction of the phase of the flow, what significantly decreases the usefulness of the model.

It is especially important in feedback control design. While small differences between phases of real flow and reduced-order model in certain instant of time can be corrected by the dynamic estimation [27], larger errors in phase prediction result in deterioration of the control effect [4].

Due to the requirement of small dimension of the model, it is not possible to overcome this problem by the computation of one POD mode basis using snapshots from all the considered flow states.

This leads to the conclusion that smooth and continuous interpolation between coherent structures, representing different flow states, is a crucial enabler of accurate reduced-order models of transient flows (like the one described in Sec. 2). Such transition can be achieved by continuous mode interpolation, described by the authors in [5, 6].

In this technique, POD modes  $\mathbf{u}_i$  are interpolated by referring to the Fredholm eigenproblem in space domain (6.1)

$$(6.1) \quad \int_{\Omega} \mathbf{A}(x, y) \mathbf{u}_i(y) dy = \lambda_i \mathbf{u}_i(x)$$

with autocorrelation function (kernel)  $\mathbf{A}$

$$(6.2) \quad \mathbf{A}^{\kappa}(x, y) = \mathbf{u}_1^{\kappa}(x) \otimes \mathbf{u}_1^{\kappa}(y) + \mathbf{u}_2^{\kappa}(x) \otimes \mathbf{u}_2^{\kappa}(y) + \dots$$

The Fredholm kernel is linearly interpolated in  $\kappa \in [0, 1]$ :

$$(6.3) \quad A^{\kappa} = A^0 + \kappa(A^1 - A^0).$$

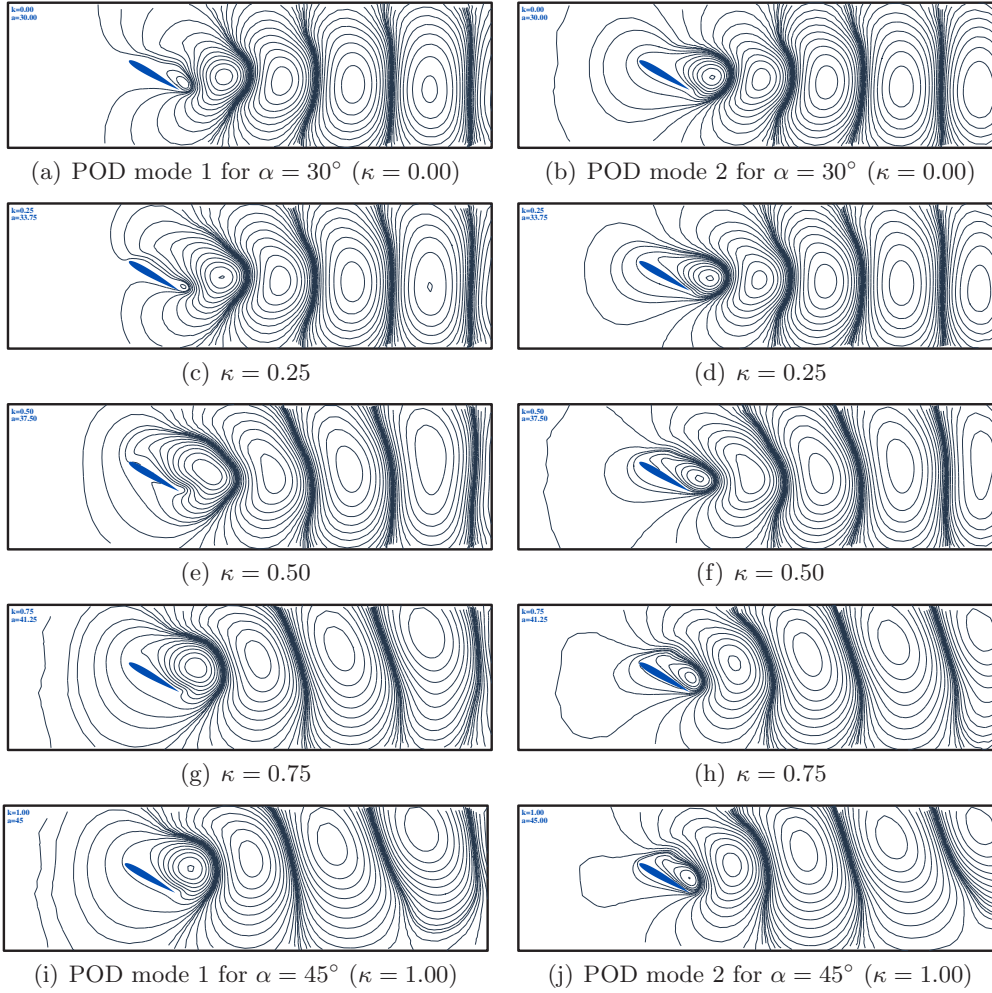


FIG. 6. Interpolated modes based on rotated domain. Top: Two most energetic POD modes for  $\alpha = 30^\circ$  (universal stream horizontal). Bottom: Two most energetic POD modes for  $\alpha = 45^\circ$  (universal stream directed  $15^\circ$  upwards). Middle: Interpolated modes for  $\kappa = 0.25$ ,  $\kappa = 0.50$  and  $\kappa = 0.75$ . In the figure, the streamlines of the modes are depicted. The comparison of POD basis for  $\alpha = 37.5^\circ$  and interpolated modes for  $\kappa = 0.50$  is given in [6].

Eigenvectors of interpolated Fredholm eigenproblem (interpolated modes)  $\mathbf{u}^\kappa$  can be used to model all the intermediate states between  $\kappa = 0$  and  $\kappa = 1$ .

In the present study,  $\kappa = 0$  describes the mode basis for  $\alpha = 30^\circ$ , while  $\kappa = 1$  is used to model the flow at  $\alpha = 45^\circ$ . To model that state, two POD mode sets are used. In the first case (Fig. 6), whole domain is rotated to get the desired angle of attack. In the second case (Fig. 7), the rotation is achieved by mesh deformation mentioned in Sec. 2.

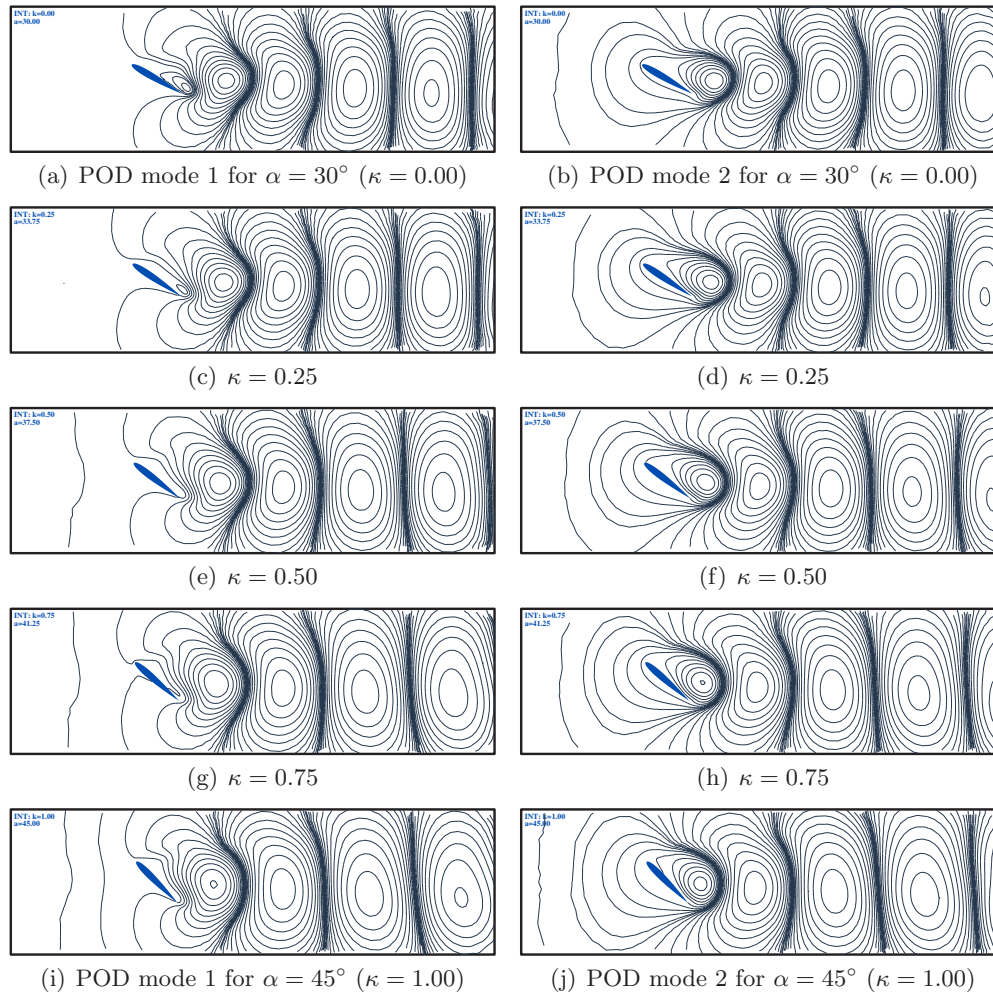


FIG. 7. Interpolated modes based on deformed mesh. Top: Two most energetic POD modes for  $\alpha = 30^\circ$ . Bottom: Two most energetic POD modes for  $\alpha = 45^\circ$ . Middle: Interpolated modes for  $\kappa = 0.25$ ,  $\kappa = 0.50$  and  $\kappa = 0.75$ . In the figure, the streamlines of the modes are depicted.

In all cases, uniform stream is horizontal.

The purpose of checking these two possibilities is to compare them and select one for further development. The rotation of whole domain is easier to achieve, but can be applied in reduced-order modelling only for single-part, rigid bodies. Additionally, the domain has to be large enough to ensure that after the rotation, the wake will not be disrupted by the boundary conditions. When the body consists of multiple moving parts (like high-lift configurations), mesh deformation is required.

Using interpolated modes  $\mathbf{u}^\kappa$ , the construction of low-dimensional model for time-varying operating conditions is possible (6.4):

$$(6.4) \quad \begin{aligned} \dot{a}_i^\kappa &= \frac{1}{\text{Re}} \sum_{j=0}^N l_{ij}^\kappa a_j^\kappa + \sum_{j=0}^N \sum_{k=0}^N q_{ijk}^\kappa a_j^\kappa a_k^\kappa, \\ \dot{\kappa} &= F(\kappa, \mathbf{a}^\kappa, t). \end{aligned}$$

During transitions from steady to time-averaged solutions, presented in [5, 6, 21],  $\kappa$  was related to shift-mode amplitude. In the present study,  $\kappa$  depends on time only, changing from  $\kappa = 0$  for  $t \leq 500$  s to  $\kappa = 1$  for  $t \geq 510$  s.

Galerkin system coefficients  $l_{ij}^\kappa$  and  $q_{ijk}^\kappa$ , depending on the parameter  $\kappa$ , are linearly interpolated between two operating conditions identified by  $\kappa = 0$  and  $\kappa = 1$ :

$$(6.5) \quad l_{ij}^\kappa = l_{ij}^0 + \kappa(l_{ij}^1 - l_{ij}^0), \quad q_{ijk}^\kappa = q_{ijk}^0 + \kappa(q_{ijk}^1 - q_{ijk}^0).$$

## 7. Reduced-order model of the flow with changing boundary conditions

In previous sections, construction of mode basis for time-varying operating conditions was presented. In this section, two 8-dimensional reduced-order models of the flow, described in Sec. 2, are presented. They use 6 interpolated POD modes and a shift mode. Eighth degree of freedom is the interpolation parameter  $\kappa$ .

Both of the models utilize the same mode set for  $\alpha = 30^\circ$  ( $\kappa = 0$ ). For  $\alpha = 45^\circ$ , the first one (“GM-1”) uses modes computed for a rotated domain (Fig. 6). The second model (“GM-2”) is based on the interpolation between modes computed for initial and deformed meshes (Fig. 7).

Figure 8 depicts the variation of total kinetic energy of the disturbance in time for DNS model (bold line) and two Galerkin models. The transition from steady solution to limit cycle for  $\alpha = 30^\circ$  shows fragility of POD models due to the change of operating conditions. The method of quality improvement at this stage, using continuous interpolation between stability eigenmodes and POD modes, is described in [21].

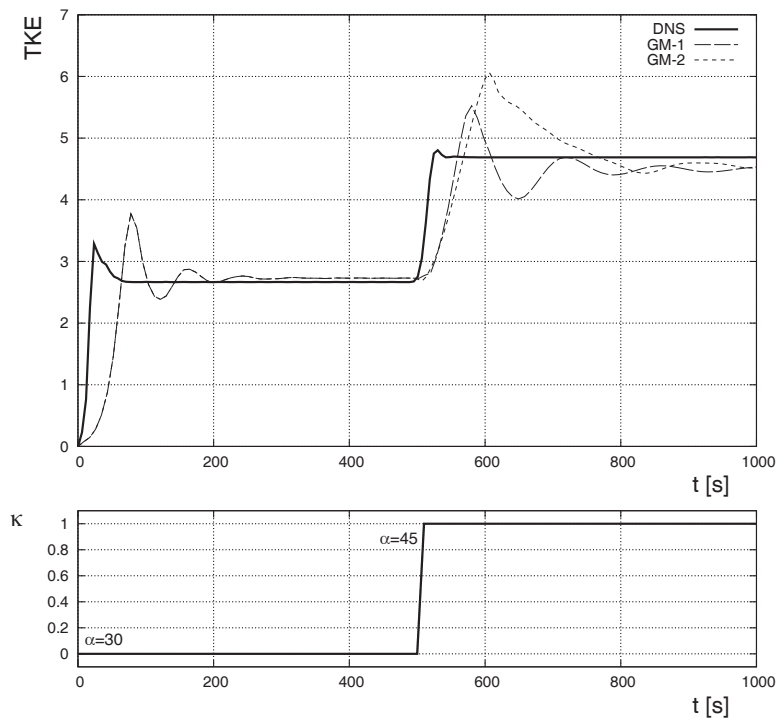


FIG. 8. Total kinetic energy of the disturbance for transition from steady state to limit cycle oscillations at angle of attack  $\alpha = 30^\circ$  and next, for transition from  $\alpha = 30^\circ$  to  $\alpha = 45^\circ$  ( $t \geq 500$  s).

The change of  $\alpha$  is done when limit-cycle oscillations are reached. It can be noticed, that the disturbance kinetic energy of both Galerkin models at  $t = 500$  s (equal to  $TKE = 2.73$ ) and the period time of limit-cycle oscillations ( $T = 6.90$  s) for  $\alpha = 30^\circ$ , are very close to the levels characterizing direct numerical simulation.

The change of angle of attack results in temporary overestimation of TKE in the case of both Galerkin models. For both the Galerkin models, the peak of energy is larger and occurs later than in the case of Navier–Stokes model. Then, the disturbance energy decreases and slowly reaches the level slightly lower than the energy of DNS. That change has different course for each of the reduced-order models: in the case of the one utilizing domain rotation, the function of TKE in time has a more oscillatory nature, while the second model (“GM-2”) is characterized by larger peak of energy. Final level of TKE (equal to 4.52) is achieved by both Galerkin models at  $t \approx 1000$  s, much later than in the case of a high-dimensional model. Compared to DNS, the TKE of Galerkin Models has an average error of 3.6%.

For second value of the angle of attack, oscillations of both Galerkin models have slightly different frequencies: for the model with rotating domain (“GM-1”) the period time is  $T = 8.26$  s, and for the model based on deformed mesh –  $T = 8.10$  s. Both these values are comparable with the period times measured from DNS.

The evaluation of Fourier coefficient values leads to the conclusion, that one of the reasons for the peak and the oscillations of disturbance kinetic energy is the behaviour of shift-mode coefficient (Fig. 9).

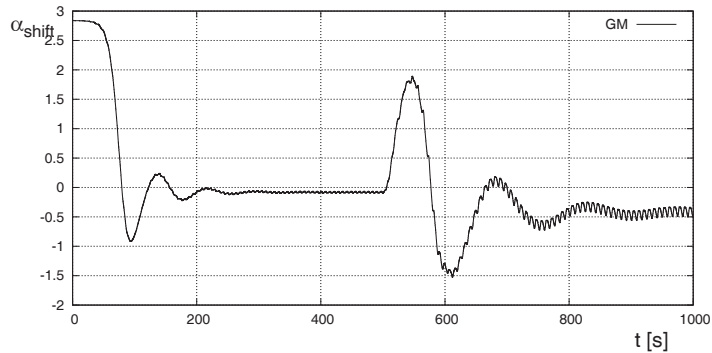


FIG. 9. Shift-mode coefficient  $a_{\text{shift}}$  for model “GM-1”.

It should be noted that the rapid growth of TKE occurs for the peak of shift-mode coefficient, and when  $a_{\text{shift}}$  reaches local minimum – the energy falls down.

While the mean flow and shift-mode are continuously interpolated just as POD modes, the considered  $a_{\text{shift}}$  coefficient is expected to be close to zero when limit-cycle oscillations are reached. Since it behaves in a different way, it might be modified externally.

Such calibration of  $a_{\text{shift}}$  value is the way to suppress the oscillations of Galerkin model’s TKE. The variation of total kinetic energy, for the test model using this approach, is presented in Fig. 10.

When the flow angle is changed slower, the adaptation of the flow pattern from ROM to new operating conditions improves – the peak of the TKE is smaller and the oscillations are damped (Fig. 10). Such a result indicates that the oscillations of the TKE and the “inertia” of POD system are related to the lack of smaller eddies in the POD basis. This behaviour might be improved by addition of the dissipative term to the Galerkin model, whose role is to mimic the energy sink caused by neglecting small-scale POD modes.

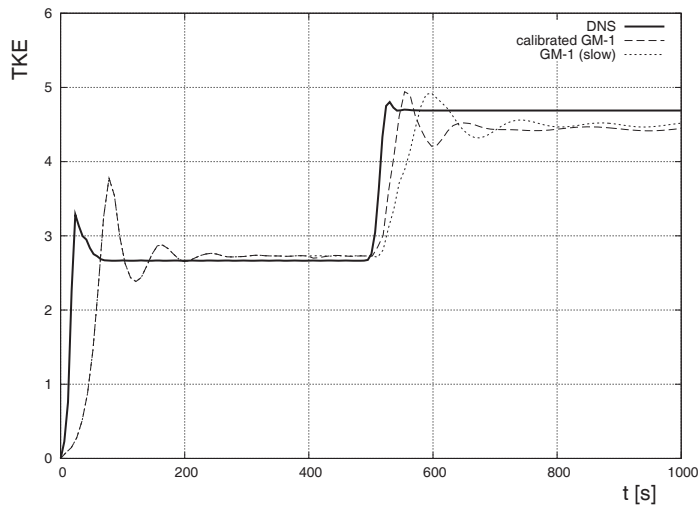


FIG. 10. Total kinetic energy of the disturbance for calibrated Galerkin model “GM-1” and for the case when the flow angle change rate is smaller.

## 8. Conclusions

In this paper, Reduced Order Galerkin Models of flow around NACA-0012 airfoil with changing angle of attack are presented. The chosen test-case represents a set of flows with varying operating and boundary conditions, that can be modelled using the Galerkin Method.

Continuous mode interpolation allows low-dimensional modelling of flow and structures that have not been computed before. In the present study, Proper Orthogonal Decomposition of limit-cycle oscillations for two distinct angles of attack  $\alpha = 30^\circ$  and  $\alpha = 45^\circ$  allows the modelling of flow for the whole range of angles between  $\alpha = 30^\circ$  and  $\alpha = 45^\circ$ .

For limit-cycle oscillations, all the models are in good agreement with Direct Numerical Simulation – both the TKE and frequencies are similar.

The models utilizing interpolated POD modes (“GM-1” and “GM-2”) tend to have oscillations of the energy after the angle has changed. This behaviour, similar to the one that occurs during transition from steady solution to periodic flow, results in deterioration of the accuracy.

The solution of this problem is the use of calibrated model, where the value of shift-mode coefficient is better matched to the DNS values. Additional possibility of such improvement is to exploit eigenmodes of global flow stability analysis and to use inertial manifold approximations [28].

In the near future, these methods and the continuous mode interpolation will be investigated on other examples of flows with varying operating and boundary

conditions. Further development, like the incorporation of 3D modes or Euler equations, will be useful in the construction of reduced-order models for aeroelastic simulations.

## Acknowledgements

This work was supported by the Deutsche Forschungsgemeinschaft (DFG) under grants NO 258/1-1, NO 258/2-3, SCHL 586/1-1 and the Bernd R. Noack Cybernetics Foundation.

We acknowledge excellent working conditions and support of DFG-funded Collaborative Research Center: the Sfb 557 “Control of complex turbulent shear flows” at the Berlin University of Technology.

The work of Gilead Tadmor was partially supported by NSF grants 0410246 and 0524070 and the US AFOSR grants FA 9550-05-1-0399 and FA 9550-06-01-0373.

## References

1. P.J. STRYKOWSKI, K.R. SREENIVASAN, *On the formation and suppression of vortex ‘shedding’ at low Reynolds numbers*, J. Fluid Mech., **218**, 71–107, 1990.
2. D.M. BUSHNELL, J.N. HEFNER, *Viscous drag reduction in boundary layers*, [in:] Progress in Aeronautics and Astronautics, **123**, AIAA, Washington, D.C.
3. J. GERHARD, M. PASTOOR, R. KING, B.R. NOACK, A. DILLMANN, M. MORZYŃSKI and G. TADMOR, *Model-based control of vortex shedding using low-dimensional Galerkin models*, [in:] 33rd AIAA Fluids Conference and Exhibits, Orlando, Florida, U.S.A., June 23–26, Paper 2003-4262.
4. B.R. NOACK, K. AFANASIEV, M. MORZYŃSKI, G. TADMOR F. THIELE, *A hierarchy of low-dimensional models for the transient and post-transient cylinder wake*, J. Fluid Mech. **497**, 335–363, 2003.
5. M. MORZYŃSKI, W. STANKIEWICZ, B.R. NOACK, F. THIELE, G. TADMOR, *Generalized mean-field model with continuous mode interpolation for flow control*, [in:] 3rd AIAA Flow Control Conference, San Francisco, Ca, USA, 5–8 June. Invited AIAA-Paper 2006-3488.
6. M. MORZYŃSKI, W. STANKIEWICZ, B.R. NOACK, R. KING, F. THIELE, G. TADMOR, *Continuous Mode Interpolation for Control-Oriented Models of Fluid Flow*, [in:] Notes on Numerical Fluid Mechanics and Multidisciplinary Design. Volume 95: Active Flow Control, R. KING [Ed.], Springer, Berlin, 260–278.
7. M. MORZYŃSKI, *Numerical solution of Navier–Stokes equations by the finite element method*, [in:] Proceedings of SYMKOM 87, Compressor and Turbine Stage Flow Path – Theory and Experiment, 119–128, 1987.
8. W. STANKIEWICZ, *Algorithm for deformation of three-dimensional flow grids* [in Polish], Zeszyty Naukowe Politechniki Poznańskiej, Maszyny Robocze i Transport, **59**, 143–148, 2005.

9. B.R. NOACK, P. PAPAS, P.A. MONKEWITZ, *Low-dimensional Galerkin model of a laminar shear-layer*, Technical Report **2002-01**, Laboratoire de Mécanique des Fluides, Département de Génie Mécanique, École Polytechnique Fédérale de Lausanne, Switzerland, 2002.
10. B.R. NOACK, P. PAPAS, P.A. MONKEWITZ, *The need for a pressure-term representation in empirical Galerkin models of incompressible shear-flows*, *J. Fluid Mech.*, **523**, 339–365, 2005.
11. F.H. BUSSE, *Numerical analysis of secondary and tertiary states of fluid flow and their stability properties*, *Appl. Sci. Res.*, **48**, 341–351, 1991.
12. R.W. PANTON, *Incompressible Flow*, John Wiley & Sons, New York 1984.
13. R. PEYRET, *Spectral Methods for Incompressible Viscous Flow*, Springer, New York 2002.
14. M. FARGE, K. SCHNEIDER, N. KEVLAHAN, *Non-Gaussianity and Coherent Vortex Simulation for two-dimensional turbulence using an adaptive orthonormal wavelet basis*, *Phys. Fluids*, **11**, 8, 2187–2201, 1999.
15. B.R. NOACK, *Niederdimensionale Galerkin-Modelle für laminare und transitionelle Scherströmungen* (transl.: *Low-dimensional Galerkin models of laminar and transitional shear-flow*), Technical report, Habilitation thesis, 2005.
16. B. RUMMLER, *Zur Lösung der instationären inkompressiblen Navier–Stokeschen Gleichungen in speziellen Gebieten*, (transl.: *On the solution of the incompressible Navier–Stokes equations in some domains*), Technical Report Habilitationsschrift, Fakultät für Mathematik, Otto-von-Guericke-Universität Magdeburg, 2000.
17. L. BOBERG, U. BROSA, *Onset of Turbulence in a Pipe*, *Z. Naturforsch.*, **43a**, 697–726, 1988.
18. P.F. BATCHO, *Global Spectral Methods for the Solution of the Incompressible Navier–Stokes Equations in Complex Geometries: The Generalized Stokes Eigensystem*, PhD thesis, Princeton University, 1994.
19. K. AFANASIEV, *Stabilitätsanalyse, niedrigdimensionale Modellierung und optimale Kontrolle der Kreiszyylinderumströmung* (transl.: *Stability analysis, low-dimensional modelling, and optimal control of the flow around a circular cylinder*), PhD thesis, Fakultät Maschinenwesen, Technische Universität Dresden, 2003.
20. M. MORZYŃSKI, K. AFANASIEV, F. THIELE, *Solution of the eigenvalue problems resulting from global non-parallel flow stability analysis*, *Comput. Meth. Appl. Mech. Engrg.*, **169**, 161–176, 1999.
21. W. STANKIEWICZ, M. MORZYŃSKI, B.R. NOACK, G. TADMOR, *Reduced Order Galerkin Models of Flow Around NACA-0012 Airfoil*, *Mathem. Modelling and Analysis*, **13**, 1, 113–122, 2008.
22. P. HOLMES, J.L. LUMLEY, G. BERKOOZ, *Turbulence, Coherent Structures, Dynamical Systems and Symmetry*, Cambridge University Press, Cambridge 1998.
23. D. REMPFER, *Kohärente Strukturen und Chaos beim laminar-turbulenten Grenzschichtumschlag* (transl.: *Coherent structures and chaos of the laminar-turbulent boundary-layer transition*), PhD theses, Fakultät Verfahrenstechnik der Universität Stuttgart, 1991 (Part of this work has been published by D. REMPFER, F.H. FAZLE, in *J. Fluid Mech.*, **260** & **275**).

24. D. REMPFER, *Empirische Eigenfunktionen und Galerkin-Projektionen zur Beschreibung des laminar-turbulenten Grenzschichtumschlags* (transl.: *Empirical eigenfunctions and Galerkin projection for the description of the laminar-turbulent boundary-layer transition*), Habilitation Thesis, Fakultät für Luft- und Raumfahrttechnik, Universität Stuttgart, 1995.
25. G. BERKOOZ, P. HOLMES, J.L. LUMLEY, *The proper orthogonal decomposition in the analysis of turbulent flows*, *Ann. Rev. Fluid Mech.*, **25**, 539–575, 1993.
26. L. SIROVICH, *Turbulence and the dynamics of coherent structures*, *Quart. Appl. Math.*, **45**, 561–590, 1987.
27. G. TADMOR, B.R. NOACK, M. MORZYŃSKI, S. SIEGEL, *Low-dimensional models for feedback flow control. Part II: Controller design and dynamic estimation*, [in:] 2nd AIAA Flow Control Conference, Portland, Oregon. U.S.A., June 28–July 1, 2004, AIAA Paper, 2004-2409 (invited contribution).
28. B.R. NOACK, M. SCHLEGEL, B. AHLBORN, G. MUTSCHKE, M. MORZYŃSKI, P. COMTE, G. TADMOR, *A finite-time thermodynamics formalism for unsteady flows*, *J. Non-Equilib. Thermodyn.*, **33** (2), 1–45, 2008.

Received June 6, 2008; revised version September 8, 2008.

---